ORIGINAL ARTICLE

# Phase-Change-Driven Dielectric-Plasmonic Transitions in Chalcogenide Metasurfaces

*Behrad Gholipour*[1, 2†], *Artemios Karvounis*[1], *Jun Yin*[3], *Cesare Soci*[3], *Kevin F. MacDonald*[1†], *and Nikolay I. Zheludev*[1, 3]

[1] *Optoelectronics Research Centre & Centre for Photonic Metamaterials, University of Southampton, SO17 1BJ, UK*

[2] *School of Chemistry, University of Southampton, Highfield, Southampton, SO17 1BJ, UK*

[3] *Centre for Disruptive Photonic Technologies, TPI, SPMS, Nanyang Technological University, 21 Nanyang Link, Singapore 637371*

[*]*Corresponding author: bg305@orc.soton.ac.uk, kfm@orc.soton.ac.uk*

**Chalcogenides – alloys based upon group-16 'chalcogen' elements (sulfur, selenium and tellurium) covalently bound to 'network formers' such as arsenic, germanium, antimony and gallium – present a variety of technologically useful properties, from infrared transparency and high optical nonlinearity to photorefractivity and readily-induced, reversible non-volatile structural phase switching. Such phase change materials are of enormous interest in the field of plasmonics and nanophotonics. For such applications, it has gone largely unnoticed however, that some chalcogenides accrue plasmonic properties in the transition from an amorphous to a crystalline state, i.e. the real part of their relative permittivity becomes negative. Indeed, one of the most commercially important chalcogenide compounds, germanium antimony telluride ($Ge_2$:$Sb_2$:$Te_5$ or GST), which is widely used in rewritable optical and electronic data storage technologies, presents exactly this behavior at wavelengths in the near-ultraviolet to visible spectral range[1]. In this work, we show that the phase transition-induced emergence of plasmonic properties in the**

**crystalline state can markedly change the optical properties of subwavelength-thickness nanostructured GST films, providing for the realization of non-volatile, reconfigurable (e.g. color-tunable) chalcogenide metasurfaces operating at visible frequencies, and thus creating opportunities for developments in non-volatile optical memory, solid state displays and all-optical switching devices.**

## Introduction

Phase-change materials have played a significant role in the evolution of active plasmonic and photonic metamaterial technologies, delivering a variety of switchable, tunable, and reconfigurable optical functionalities through hybridization with plasmonic metal nanostructures[2-8]. Chalcogenides in particular, which can be electrically and optically switched between amorphous and crystalline states with markedly different electronic and photonic properties[9], have facilitated the realization of active plasmonic metamaterial devices for a variety of applications including electro- and all-optical signal switching, polarization modulation, beam steering, and multispectral imaging[10-18]. Moreover, the near-infrared high refractive index and index contrast between phase states within GST have recently been harnessed in the demonstration of laser-rewritable and optically switchable nanostructured 'all-dielectric' (i.e. all-chalcogenide) metasurfaces[19-21]. At the same time, several bulk monocrystalline chalcogenides have been recognized as 'topological insulators' (TI's) – semiconductors with topologically-protected metallic surface states arising through strong spin-orbit interactions[7,22,23]. Indeed, the quaternary TI alloy $Bi_{1.5}Sb_{0.5}Te_{1.8}Se_{1.2}$ (BSTS) has recently been demonstrated as a UV-visible range plasmonic medium.[24]

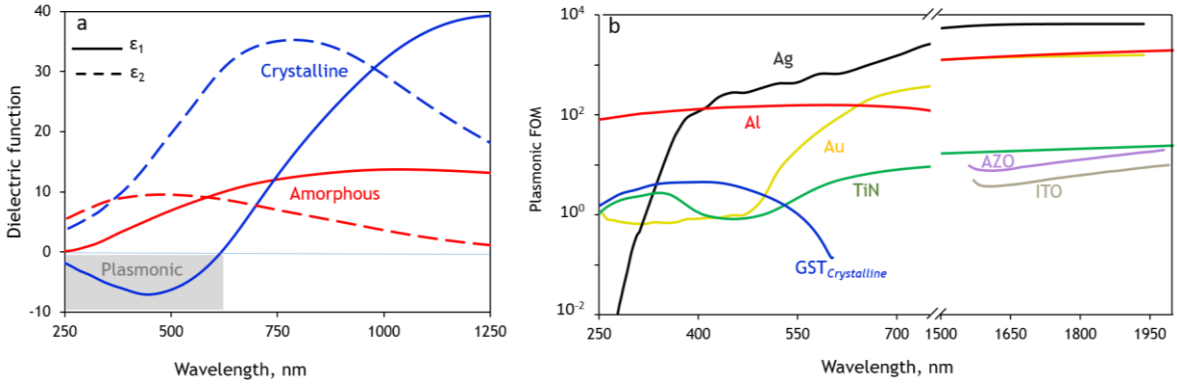


**Figure 1: Chalcogenide plasmonics.** (a) Spectral dispersion [from variable angle ellipsometric measurements] of the real $\varepsilon_1$ and imaginary $\varepsilon_2$ parts of the relative permittivity of sputtered germanium antimony telluride [GST] in its amorphous and polycrystalline phases. (b) Spectral dispersion of plasmonic figure of merit for polycrystalline GST and a selection of other plasmonic materials [as labelled; calculated using material parameters from[6,7,23,25].

Here we show that thin film GST can be optically switched between amorphous and polycrystalline states which, at UV/VIS wavelengths, are respectively dielectric and metallic (i.e. plasmonic), and demonstrate this in the context of switchable photonic metasurfaces. The real part $\varepsilon_1$ of relative permittivity (**Figure 1a**) for polycrystalline GST has a negative value, as is required for a medium in air/vacuum to support surface plasmons[26], at wavelengths $\lambda$ below 660 nm, and a positive value at longer wavelengths. In contrast, amorphous GST is a dielectric, with a positive value of $\varepsilon_1$, across the entire ultraviolet to near-infrared spectral range. **Figure 1b** presents the plasmonic figure of merit $Re\{k_{SPP}\}/2\pi Im\{k_{SPP}\}$ – the surface plasmon polartiton (SPP) propagation decay length in units of SPP wavelength[27] – for polycrystalline GST alongside a number of other, noble metal and recently-proposed alternative[28], plasmonic media. ($k_{SPP} = k_0\sqrt{\varepsilon_m\varepsilon_d/(\varepsilon_m + \varepsilon_d)}$ being the wavevector of surface plasmon polaritons on a planar interface between metallic and dielectric media with complex relative permittivities $\varepsilon_m$ and $\varepsilon_d$ respectively; The latter is taken to be air in the present case; $k_0$ is the free space wavevector.) On this basis, GST is comparable if not superior to most other materials in the

UV-to-blue/green visible wavelength range, with the exception of Al, and almost as good a plasmonic medium in this spectral band as highly-doped transparent conductive oxides are at near-infrared wavelengths.

Standalone, optically thick GST is an absorbing medium at ultra-violet/visible wavelengths, with a reflectivity that is substantially modified, yielding vibrant color in this spectral range through the introduction of nano-grating structures, when illuminated with light with a polarization perpendicular to the nanogratings (TM) **(Figure S1)**. In order to achieve reversible optical switching in practical devices, the film needs to be thin (semi-transparent) and encapsulated between transparent protective layers to prevent degradation of the chalcogenide in air, especially at elevated phase transition temperatures[10]. Encapsulation of a sub-wavelength GST film between two transparent ZnS/SiO2 films gives rise to the appearance of a broad drop in reflection and transmission as a result of Fabry-Perot type interference between the central high index absorbing film and its lower index protective layers[29], with the amorphous-crystalline transition only producing a broadband change in the level of reflection/transmission in the unstructured case.

## Materials and Methods

For the present study, 70 nm of GST was deposited between 70 nm protective layers of $ZnS/SiO_2$ on optically flat quartz substrates by RF sputtering (Kurt J. Lesker Nano 38) from $Ge_2Sb_2Te_5$ and $ZnS:SiO_2$ (1:9) alloy targets. A base pressure of $5 \times 10^{-7}$ mbar was achieved prior to deposition and high-purity argon was used as the sputtering gas. The substrate was held within 10K of room temperature on a rotating platen 150 mm from the target to produce low-

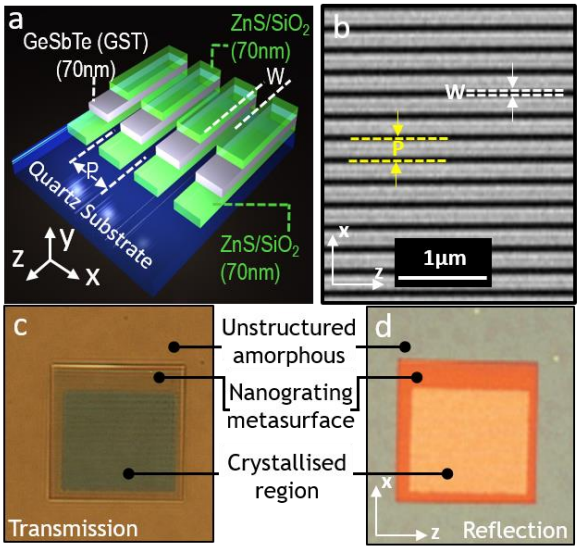


**Figure 2: GST metasurfaces.** (a) Artistic cut-away section of nano-grating metasurface structures fabricated in a 70 nm film of GST between two layers [70 nm each] of $ZnS/SiO_2$. (b) Scanning electron microscope image of a section of a $ZnS/SiO_2$–GST–$ZnS/SiO_2$ tri-layer metasurface [dark areas being the quartz substrate exposed by focused ion beam milling, i.e. removal of the tri-layer]. (c) Transmission and (d) reflection TM-polarized, normal incidence reflection images of a 20 × 20 µm, $P$ = 400 nm, amorphous phase GST tri-layer metasurface domain [surrounded by unstructured amorphous phase GST tri-layer], part of which – the central 12 × 12 µm region appearing green in transmission, pale orange in reflection – has been selectively crystallized by fs-pulsed laser illumination.

stress amorphous films. Nano-grating metasurface arrays were subsequently milled though the $ZnS/SiO_2$–GST–$ZnS/SiO_2$ tri-layer using a focused (gallium) ion beam (FEI Helios NanoLab 600), at beam currents ≤28 pA to prevent crystallization of GST (via ion beam-induced heating) during the milling process. Metasurface domains, each measuring 20 × 20 µm in the sample plane, were fabricated with a range of periods $P$ from 250nm to 400 nm, with a fixed milled linewidth $W$ of 100 nm (**Figure 2**).

The amorphous-to-crystalline transition in chalcogenides is an annealing process that may be initiated globally by ambient, or locally by laser- or electrical current-induced heating to a temperature above the material's glass-transition point $T_g$ (~160°C for GST) but below its melting point $T_m$ (~600°C)[30]. The reverse transition – a melt-quenching process – can be driven

by shorter, higher energy pulsed excitations that bring the material momentarily to a temperature above $T_m$ [31]. In this work, structural transitions in the GST layer are excited using 85 fs laser pulses at a wavelength of 730 nm in a beam focused to a diffraction-limited spot and raster-scanned over the sample using a spatial light modulator, as described in Ref. [32]. By varying the number, repetition rate and energy of pulses delivered at a given point, one may accurately control the temporal profile of optically-induced temperature change in the GST. Here, we employed trains of fifty ~140 $mJ.cm^{-2}$ pulses at a repletion rate of 1 MHz for crystallization.

The normal-incidence transmission and reflection characteristics of the GST nano-grating metasurfaces, in amorphous and crystalline states, were quantified, for incident polarizations perpendicular and parallel to the grating lines (along the *x* and *z* directions defined in **Figure 2**, or TE and TM orientations of the grating, respectively), using a microspectrophotometer (CRAIC QDI2010) with a sampling domain size of 15 μm x 15 μm and numerical aperture of 0.28.

## Results and Discussion

With GST in its amorphous phase, the transmission of the unstructured $ZnS/SiO_2$–GST–$ZnS/SiO_2$ tri-layer increases monotonically with wavelength across the UV to near-IR spectral range, from around 5% at 400 nm to 35% at 900 nm (**Figure 3a**). For the polycrystalline phase, levels of transmission are suppressed across the entire range but follow essentially the same trend, reaching approximately 12% at 900 nm (**Figure 3b**). The sub-wavelength period (and therefore non-diffractive) nano-grating metasurface structures introduce resonances for TM-polarized light (incident electric field perpendicular to the grating lines), at visible wavelengths dependent on period *P*, for both phase states of GST, which manifest themselves in the

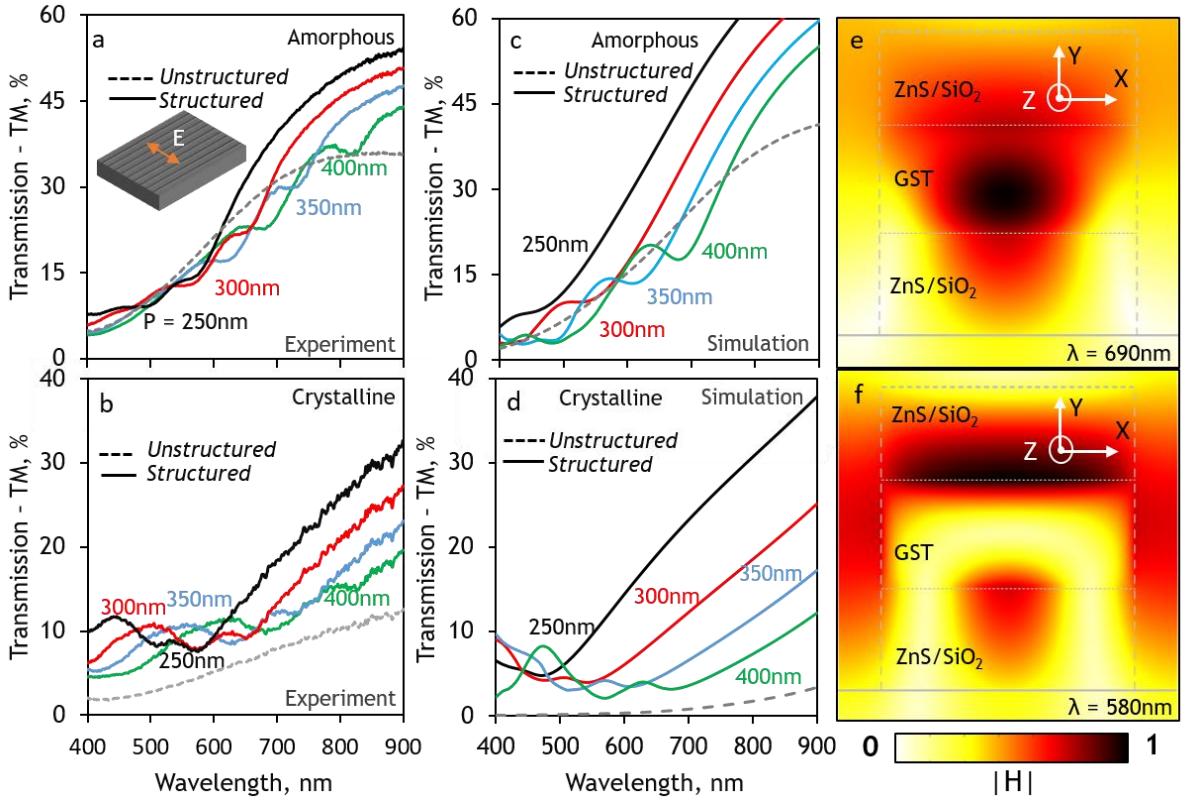


**Figure 3: Optical properties of amorphous [dielectric] and polycrystalline [plasmonic] GST metasurfaces.** (a, b) Measured spectral dispersion of $ZnS/SiO_2$–GST–$ZnS/SiO_2$ nano-grating metasurface TM transmission for a selection of grating periods *P* [as labelled], for the amorphous (a) and polycrystalline (b) states of the GST layer, overlaid with spectra for the unstructured tri-layer [dashed lines]. Corresponding numerically simulated transmission spectra (c, d). Distributions of the normalized magnetic field, H in the *xz*-plane for a unit cell of a *P* = 400 nm nano-grating (e, f) for transmission resonance wavelength at $\lambda$ = 580nm for amorphous and 690nm for the respective crystalline phase.

transmitted and reflected colors of the metamaterial domains **(Figures 2c-d)**. Due to the highly anisotropic nature of nanograting resonators and the plasmonic nature of the GST layer, the optical response depends on the polarization of incident light. As such, the observed response of the nanograting metasurfaces is highly sensitive to polarization, with resonant peaks disappearing with incident polarization parallel to the grooves of the grating (TE). In this orientation the nano-grating behaves as a linear medium with a non-dispersive effective refractive index related to that of the $ZnS/SiO_2$-GST-$ZnS/SiO_2$ stack and its fill fraction within

the grating structure. Therefore, for TE-polarized light, the observed optical response in either amorphous or polycrystalline GST is largely invariant with nano-grating period and almost identical to the unstructured tri-layer transmission spectrum for the corresponding phase state. (Corresponding reflection spectra, and TE polarized spectra are presented in **Figure S2 & S3**).

It should be noted that the observed TM resonances are of markedly different nature for the two phase states of GST – in the amorphous case they are displacement current resonances reliant upon the high refractive index contrast between the dielectric GST and surrounding media, while for the crystalline phase the resonances are plasmonic, i.e. based upon the opposing signs of $\varepsilon_1$ at interfaces between the GST and surrounding media. Numerical simulations clearly illustrate this difference: **Figures 3c-f** show results of a 3D finite-element Maxwell solver model, which employs ellipsometrically measured values for the complex permittivity of GST as presented in **Figure 1a**. It assumes lossless non-dispersive refractive indices of 1.46 and 1.80 for the semi-infinite quartz substrate and the $ZnS/SiO_2$ layers respectively; normally-incident narrowband plane wave illumination; and, by virtue of periodic boundary conditions, a nano-grating pattern of infinite extent in the *x-y* plane. There is good qualitative and quantitative agreement between experimentally measured (**Figure 3a, b**) and numerically simulated (**Figs. 3c, d**) transmission spectra for the GST metasurfaces in both amorphous and crystalline states. Discrepancies are attributed to manufacturing imperfections (the computational model assumes ideal rectilinear nano-grating geometry as illustrated schematically in **Figure 2a)** and contamination of the $ZnS/SiO_2$ and GST layers (gallium ion implantation) during FIB milling, which can have the effect of slightly modifying refractive

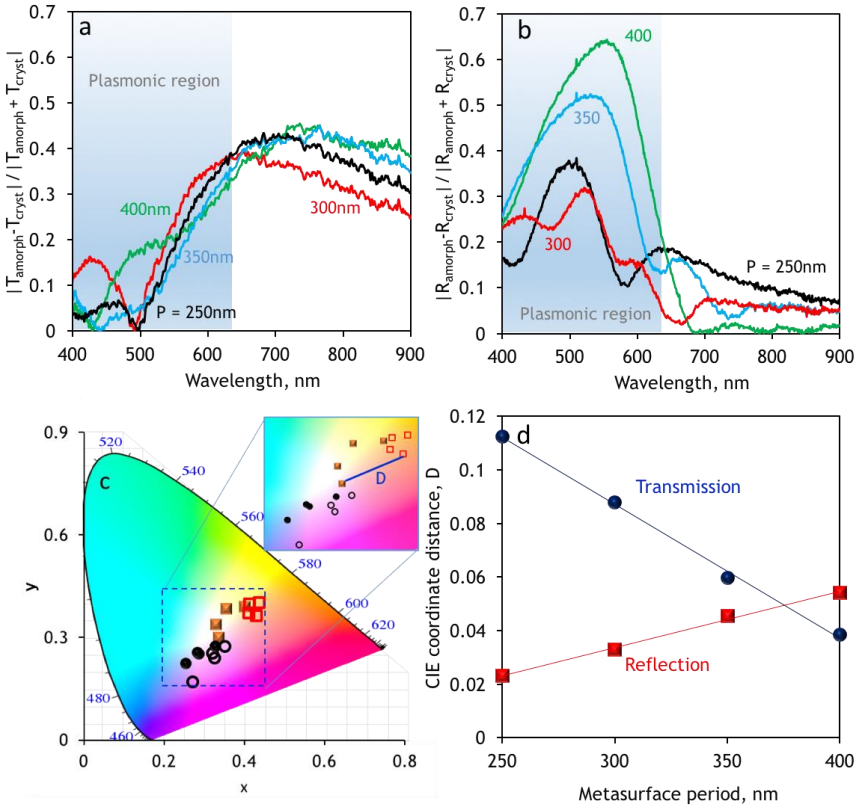


**Figure 4: Swiching contrast and color change.** Relative (a) transmission and (b) reflection change induced by (upon) structural change between amorphous and crystalline phases of the GST metasurfaces with different periods (as labeled). (c) Corresponding reflection (circles) and transmission (squares) CIE color palette with marked points indicating the metasurfaces [$P$ = 250 – 400 nm] shown for both amorphous (unfilled) and crystalline (filled) phases. (d) Color change resulting from phase transition quantified as the Euclidean distance [D] in CIE color plot between corresponding amorphous and crystalline points, given as a function of metamaterial period.

index. The cross-sectional distributions of magnetic field in **Figures 3e and 3f**, reveal essential differences between the resonant modes for amorphous and crystalline phase of GST: in the former case the field is stronger within the (higher index dielectric) GST layer than in the $ZnS/SiO_2$ layers above and below, while in the latter the field is 'expelled' from the body of the metallic GST layer and is stronger at the interfaces with $ZnS/SiO_2$.

Non-volatile, light-induced structural transitions between amorphous and crystalline phases of GST, i.e. its conversion between dielectric and plasmonic states, thereby changes the transmission and reflection characteristics of the metamaterial, manifested in the visible

spectral range as changes in color. We define the transmission and reflection switching contrast as a ratio of the difference between levels for the amorphous and crystalline phases of the GST layer to the sum of said levels (**Figures 4a, b**). In the present case, greatest contrast is achieved in reflection, at grating period-dependent wavelengths in the spectral band where GST is converted between dielectric and plasmonic forms. The associated changes in color can be quantified through observing the CIE 1931 color space. Perceived color coordinates for GST tri-layer metasurfaces in their amorphous and crystalline phases, derived directly from reflection and transmission spectra (using Judd-Vos-modified CIE 2-deg color matching functions[33], assuming in all cases an illuminating light source with the spectral radiant power distribution of a 6500 K black body and a normalized observational brightness level) are plotted in a two-dimensional representation of the CIE1931 space in **Figure 4c**. The change in color brought about by the structural transition in GST can be quantified as the Euclidean distance between corresponding points in CIE space **(Figure 4d)**, and is found remarkably to be a linear function of metasurface period *P* in both transmission and reflection: the magnitude of the color change, in these terms, increases with period in reflection, and decreases with period in transmission. From a physical point of view, in the demonstrated metasurfaces, as period of the metasurface increases, both reflection and transmission resonances red-shift & a lowering in their Q-factor is observed. This arises as the resonances move further into a spectral range where GST is progressively less plasmonic. In GST, the amorphous to crystalline phase transition brings about an overall increase in reflection and a lowering in transmission. So as the reflection resonance dips exhibit a lower Q-factor with increasing period and an overall increase in the reflection level upon crystallization, the average change (between amorphous and crystalline spectra for a given period) in reflection increases with period. In contrast for transmission, at

lower period, due to the more plasmonic nature of the GST, higher q-factor resonance peaks are observed that are damped out with increasing period reducing the average change in transmission and consequently reducing the observed change in color in the CIE plot.

In summary, we show that the chalcogenide phase-change medium, germanium antimony telluride (GST), can be switched in a non-volatile fashion between amorphous and crystalline phases of respectively dielectric (positive real part of relative permittivity $\varepsilon$) and metallic (negative real part of $\varepsilon$) character in the UV-visible spectral range. This behavior enables switching between plasmonic and all-dielectric resonances in nanostructured GST, in a sub-wavelength optically switchable device geometry. Phase change chalcogenides have been touted as a potential candidate for future solid-state displays. To obtain the color gamut required for these applications, research has focused on complex multilayer deposition or nanofabrication procedures or hybridisation with metallic back reflectors[34-36].

As opposed to coloring achieved by multilayer depositions, the vibrant coloring observed from nanograting metasurfaces **(Figure 2, 4, S1)** is completely determined by structural design, and can be made dependent or independent on the polarization of incident light by the choice of metamolecule geometry (e.g use of square pillars or nano-disk designs), allowing the realisation of a wide range of color with one fabricated sample, nanostructured with different precisely designed metasurfaces. This is in contrast to the multilayer deposition techniques where for every color variation an entirely new sample has to be deposited as the color change depends on the thickness of the low index spacer[37]. Subwavelength nanostructuring can be used in conjunction with thin-film interference techniques and when optimized through adjusting the thickness of each layer absorptive, transmissive or reflective devices can be realized[38].

Among material platforms used for metamaterials, chalcogenides offer a unique compositional variety. In this work, for the purpose of this proof-of-principle demonstration, we have chosen the most commonly used GST composition ($Ge_2$:$Sb_2$:$Te_5$), however, GST and more broadly chalcogenides in particular offer a unique compositional variety (i.e. range and variability of material parameters) upon a change in stoichiometry, offering the possibility of improved losses and change in index with a change in composition[39]. Furthermore, they are capable of providing high-index dielectric, 'epsilon-near-zero' (ENZ) or topological insulator properties when the constituent elements are combined in the right proportion.

In the metal-free phase change metasurfaces demonstrated here, the magnitude of the color change is not a direct function of switching contrast, as a change in color involves an overall redistribution of the spectral response. However, plasmonic-to-dielectric transitions in such metasurfaces allow engineering controlled spectral redistributions that rely on the linear dependence of metasurface period to magnitude of color change in both reflection and transmission. The parameter space for metasurface design is large and different structural designs can extend the accessible color range beyond those demonstrated here, giving several extra degrees of freedom in the design of future phase change color pixels. Furthermore, such metasurfaces can be produced over large areas through structuring techniques such as nano-imprint lithography, micro-contact printing or nano-embossing. These low cost, fast, mass manufacturing alternatives to ion beam milling and reactive etching techniques, will also minimise process related degradation and contamination in the active phase change layer.

Consequently, such color tunable metasurfaces offer a robust CMOS-compatible material platform for active and reconfigurable metadevices such as thin solid state displays, data storage, switchable/tunable filters, beam shapers and optical limiting components.

## Conflict of Interest

The authors declare no conflict of interest.

## Acknowledgements

The work is supported by the UK Engineering and Physical Sciences Research Council [grant EP/M009122/1] and the Ministry of Education, Singapore [grant MOE2011-T3-1-005]. Following a period of embargo, the data from this paper can be obtained from the University of Southampton ePrints research repository.

## Author Contributions

BG generated the idea and designed and carried out the experiments. AK performed the modelling. CS and JY performed DFT modelling. All authors contributed to the interpretation of the results. BG, NIZ and KFM wrote the manuscript. NIZ supervised the work.

## References

1 Shportko, K., Kremers, S., Woda, M., Lencer, D., Robertson, J. & Wuttig, M. Resonant bonding in crystalline phase-change materials. Nat. Mater 7, 653-658 (2008).

2 MacDonald, K. F., Krasavin, A. V. & Zheludev, N. I. Optical modulation of surface plasmon-polariton coupling in a gallium/aluminium composite. Optics Communications 278, 207-210 (2007).

3 Driscoll, T., Kim, H.-T., Byung-Gyu, C., Kim, B.-J., Lee, Y.-W., Jockerst, M. N., Palit, S., Smith, D. R., Di Ventra, M. & Basov, D. N. Memory Metamaterials. Science 325, 1176580 (2009).

4 Dicken, M. J., Aydin, K., Pryce, I. M., Sweatlock, L. A., Boyd, E. M., Walavalkar, S., Ma, J. & Atwater, H. A. Frequency tunable near-infrared metamaterials based on VO2 phase transition. Opt. Express 17, 18330 (2009).

5 Sámson, Z. L., MacDonald, K. F., De Angelis, F., Gholipour, B., Knight, K., Huang, C. C., Di Fabrizio, E., Hewak, D. W. & Zheludev, N. I. Metamaterial electro-optic switch of nanoscale thickness. Appl. Phys. Lett. 96, 143105 (2010).

6 Rakić, A. D. Algorithm for the determination of intrinsic optical constants of metal films: application to aluminum. Applied Optics 34, 4755 (1995).

7 Pflüger, J., Fink, J., Weber, W., Bohnen, K. P. & Crecelius, G. Dielectric properties ofTiCx,TiNx,VCx, andVNxfrom 1.5 to 40 eV determined by electron-energy-loss spectroscopy. Phys. Rev. B 30, 1155-1163 (1984).

8 Ahmadivand, A., Gerislioglu, B., Sinha, R., Karabiyik, M. & Pala, N. Optical Switching Using Transition from Dipolar to Charge Transfer Plasmon Modes in Ge2Sb2Te5 Bridged Metallodielectric Dimers. Scientific Reports 7, 42807 (2017).

9 Lee, T. H. & Elliott, S. R. The Relation between Chemical Bonding and Ultrafast Crystal Growth. Advanced Materials 29, 1700814 (2017).

10 Gholipour, B., Zhang, J., MacDonald, K. F., Hewak, D. W. & Zheludev, N. I. An All-Optical, Non-volatile, Bidirectional, Phase-Change Meta-Switch. Adv. Mater 25, 3050-3054 (2013).

11 Michel, A.-K. U., Chigrin, D. N., Maß, T. W. W., Schönauer, K., Salinga, M., Wuttig, M. & Taubner, T. Using Low-Loss Phase-Change Materials for Mid-Infrared Antenna Resonance Tuning. Nano Letters 13, 3470-3475 (2013).

12 Chen, Y. G., Kao, T. S., Ng, B., Li, X., Luo, X. G., Luk'yanchuk, B., Maier, S. A. & Hong, M. H. Hybrid phase-change plasmonic crystals for active tuning of lattice resonances. Opt. Express 21, 13691 (2013).

13 Tittl, A., Michel, A.-K. U., Schaeferling, M., Yin, X., Gholipour, B., Cui, L., Wuttig, M., Taubner, T., Neubrech, F. & Giessen, H. A Switchable Mid-Infrared Plasmonic Perfect Absorber with Multispectral Thermal Imaging Capability. Adv. Mater. (2015).

14 Rude, M., Pello, J., Simpson, R. E., Osmond, J., Roelkens, G., van der Tol, J. J. G. M. & Pruneri, V. Optical switching at 1.55 um in silicon racetrack resonators using phase change materials. Appl. Phys. Lett. 103, 141119 (2013).

15 Cao, T., Zheng, G., Wang, S. & Wei, C. Ultrafast beam steering using gradient Au- Ge_2Sb_2Te_5 -Au plasmonic resonators. Optics Express 23, 18029 (2015).

16 Cao, T., Zhang, L., Simpson, R. E. & Cryan, M. J. Mid-infrared tunable polarization-independent perfect absorber using a phase-change metamaterial. Journal of the Optical Society of America B 30, 1580 (2013).

17 Wuttig, M., Bhaskaran, H. & Taubner, T. Phase-change materials for non-volatile photonic applications. Nat. Photon 11, 465-476 (2017).

18 Raeis-Hosseini, N. & Rho, J. Metasurfaces Based on Phase-Change Material as a Reconfigurable Platform for Multifunctional Devices. Materials 10, 1046 (2017).

19 Wang, Q., Rogers, E. T. F., Gholipour, B., Wang, C.-M., Yuan, G., Teng, J. & Zheludev, N. I. Optically reconfigurable metasurfaces and photonic devices based on phase change materials. Nat. Photon 10, 60-65 (2015).

20 Karvounis, A., Gholipour, B., MacDonald, K. F. & Zheludev, N. I. All-dielectric phase-change reconfigurable metasurface. Appl. Phys. Lett. 109, 051103 (2016).

21 Chu, C. H., Tseng, M. L., Chen, J., Wu, P. C., Chen, Y.-H., Wang, H.-C., Chen, T.-Y., Hsieh, W. T., Wu, H. J., Sun, G. & Tsai, D. P. Active dielectric metasurface based on phase-change medium. Laser & Photonics Reviews 10, 986-994 (2016).

22 Zhang, H., Liu, C.-X., Qi, X.-L., Dai, X., Fang, Z. & Zhang, S.-C. Topological insulators in Bi2Se3, Bi2Te3 and Sb2Te3 with a single Dirac cone on the surface. Nat. Phys 5, 438-442 (2009).

23 Werner, W. S. M., Glantschnig, K. & Ambrosch-Draxl, C. Optical Constants and Inelastic Electron-Scattering Data for 17 Elemental Metals. Journal of Physical and Chemical Reference Data 38, 1013-1092 (2009).

24 Yin, J., Krishnamoorthy, H. N. S., Adamo, G., Dubrovkin, A. M., Chong, Y., Zheludev, N. I. & Soci, C. Plasmonics of topological insulators at optical frequencies. NPG Asia Materials 9, e425 (2017).

25 Johnson, P. B. & Christy, R. W. Optical Constants of the Noble Metals. Phys. Rev. B 6, 4370-4379 (1972).

26 Barnes, W. L., Dereux, A. & Ebbesen, T. W. Surface plasmon subwavelength optics. Nature 424, 824-830 (2003).

27 Dastmalchi, B., Tassin, P., Koschny, T. & Soukoulis, C. M. A New Perspective on Plasmonics: Confinement and Propagation Length of Surface Plasmons for Different Materials and Geometries. Adv. Opt. Mater 4, 177-184 (2015).

28 Naik, G. V., Shalaev, V. M. & Boltasseva, A. Alternative Plasmonic Materials: Beyond Gold and Silver. Advanced Materials 25, 3264-3294 (2013).

29 Kats, M. A., Blanchard, R., Genevet, P. & Capasso, F. Nanometre optical coatings based on strong interference effects in highly absorbing media. Nat. Mater 12, 20-24 (2012).

30 Orava, J., Greer, A. L., Gholipour, B., Hewak, D. W., Smith, C. E., Loke, D., Lee, T. H., Wang, W. J., Shi, L. P., Zhao, R., Yeo, Y. C., Chong, T. C. & Elliott, S. R. Characterization of supercooled liquid Ge2Sb2Te5 and its crystallization by ultrafast-heating calorimetry. Nat Mater 11, 279-283 (2012).

31 Liu, Y., Aziz, M. M., Shalini, A., Wright, C. D. & Hicken, R. J. Crystallization of Ge2Sb2Te5 films by amplified femtosecond optical pulses. J. Appl. Phys. 112, 123526 (2012).

32 Wang, Q., Maddock, J., Rogers, E. T. F., Roy, T., Craig, C., Macdonald, K. F., Hewak, D. W. & Zheludev, N. I. 1.7 Gbit/in.2 gray-scale continuous-phase-change femtosecond image storage. Appl. Phys. Lett. 104, 121105 (2014).

33 Vos, J. J. Colorimetric and photometric properties of a 2° fundamental observer. Color Research & Application 3, 125-128 (1978).

34 Hosseini, P., Wright, C. D. & Bhaskaran, H. An optoelectronic framework enabled by low-dimensional phase-change films. Nature 511, 206-211 (2014).

35 Schlich, F. F., Zalden, P., Lindenberg, A. M. & Spolenak, R. Color Switching with Enhanced Optical Contrast in Ultrathin Phase-Change Materials and Semiconductors Induced by Femtosecond Laser Pulses. ACS Photonics 2, 178-182 (2015).

36 Dong, W., Qiu, Y., Yang, J., Simpson, R. E. & Cao, T. Wideband Absorbers in the Visible with Ultrathin Plasmonic-Phase Change Material Nanogratings. Jour. Phys. Chem C 120, 12713-12722 (2016).

37 Ríos, C., Hosseini, P., Taylor, R. A. & Bhaskaran, H. Color Depth Modulation and Resolution in Phase-Change Material Nanodisplays. Advanced Materials 28, 4720-4726 (2016).

38 Hägglund, C., Apell, S. P. & Kasemo, B. Maximized Optical Absorption in Ultrathin Films and Its Application to Plasmon-Based Two-Dimensional Photovoltaics. Nano Letters 10, 3135-3141 (2010).

39 Michel, A.-K. U., Wuttig, M. & Taubner, T. Design Parameters for Phase-Change Materials for Nanostructure Resonance Tuning. Adv. Opt. Mater 5, 1700261 (2017).